processes

MDPI

Article

Multielectrode Advanced Oxidation Treatment of Tannery Wastewater: Mass Transfer Characterization, Process Performance, Kinetic Modeling, and Energetic Analysis

Niswah Nafiat, Mohd Usman Mohd Junaidi, Mohd Azlan Hussain, Mohamad Fairus Rabuni, Adeline Seak May Chua and Faidzul Hakim Adnan *

Sustainable Process Engineering Centre (SPEC), Department of Chemical Engineering, Faculty of Engineering, Universiti Malaya, Kuala Lumpur 50603, Malaysia
* Correspondence: faidzulhakim.adnan@um.edu.my

Abstract

Tannery wastewater from textile-related industries poses treatment challenges due to its high load of recalcitrant pollutants. Various advanced hybrid treatments, such as electro-oxidation (EO), have been proposed but mainly focus on electrode material development. Several studies on EO using multiple electrode pairs with large electroactive surface areas exist, however, none have reported on mass transfer characterization. This study addresses these gaps by investigating the electro-degradation performance of active (mixed-metal oxide, MMO) and non-active (boron-doped diamond, BDD) anodes paired with carbonaceous (graphite) and non-carbonaceous (stainless steel, SS) cathodes under applied current densities of 2 to 6 mA/cm^2. A 2 L volume of simulated tannery wastewater containing recalcitrant tannic acid was treated using three electrode pairs with a total surface area of 500 cm^2. Results showed optimal condition was identified at 4 mA/cm^2 across all electrode combinations and better degradation using BDD anodes and SS cathodes, with total organic carbon (TOC) removed up to 500 mg/L (98% removal). Adopting the 3-electrode configuration, mass transfer coefficients ranged from 4.15 to 5.18 $\times$ 10^{-6} m/s. Energy consumption evaluation suggested MMO as a more cost-effective option, while BDD remained preferable for highly recalcitrant waste. Higher currents show diminishing returns due to mass transfer and parasitic reactions.

Keywords: advanced oxidation process; electrochemical oxidation; electro-oxidation; industrial wastewater; multielectrode pairings; multiple electrode; tannery wastewater

Check for updates

Academic Editor: Maria Jose Martin de Vidales

Received: 6 November 2025
Revised: 20 December 2025
Accepted: 31 December 2025
Published: 6 January 2026

Copyright: © 2026 by the authors. Licensee MDPI, Basel, Switzerland. This article is an open access article distributed under the terms and conditions of the Creative Commons Attribution (CC BY) license.

1. Introduction

Tannery wastewater is characterized by its high load of persistent organic pollutants, including tannic acid, synthetic dyes, and a range of heavy metals, all of which pose serious environmental risks if not adequately treated [1,2]. Among these, tannic acid, a polyphenolic compound commonly used in the leather tanning process, has gained attention due to its recalcitrant nature and resistance to conventional physical, chemical, and biological treatment methods [3–5]. Tannic acid is primarily generated by leather-processing and textile industries, as well as various agro-industrial sectors such as pulp and paper mills, cork processing, olive oil production, wineries, and coffee processing facilities [6]. As environmental regulations become increasingly stringent, there is a growing demand for advanced treatment technologies that are both efficient and sustainable for the removal of such pollutants.

Electrochemical advanced oxidation processes (EAOPs), particularly electro-oxidation (EO), have emerged as promising alternatives for treating complex, recalcitrant industrial effluents [7,8]. EO is highly effective in degrading non-biodegradable organic compounds through the generation of potent oxidizing agents, such as hydroxyl radicals, directly at the anode surface or indirectly in the bulk solution [9]. The performance of EO systems is strongly influenced by several factors, including the type of electrode materials used and the applied current density, both of which determine the efficiency of radical generation, the extent of parasitic side reactions (e.g., oxygen evolution), and overall energy consumption [10,11].

Research on EAOP techniques for tannery wastewater dates back at least to the early 2000s, where studies applied EO and electro-coagulation (EC) to synthetic tannery effluents, reporting effective removal of tannins and other pollutants [12,13]. Ten years later, Costa et al. also evaluated the performance of EO treatment on a chloride-free medium, confirming the feasibility of the technologies [14]. Since then, EO (including EC, electro-Fenton (EF), and related processes) have been continuously researched and refined, giving the technology a research history of over two decades. Lately, the application has been explored on real tannery effluents to evaluate true removal efficiencies, identify matrix effects that can inhibit the process, and assess operational parameters under realistic loads. Moreover, most studies involving real effluent have been conducted using only a single electrode pair, and several EO investigations have similarly adopted this configuration but have consistently demonstrated strong capability in degrading dyes, phenolic compounds, and various ionic pollutants [15–17].

A well-known limitation of EO treatment is its high energy consumption. Many studies have attempted to reduce this issue through various approaches, such as integrating EO with other processes to create hybrid treatment systems that lower the pollutant load, or by optimizing operating conditions. These optimization efforts typically involve selecting more efficient electrode materials and fine-tuning parameters such as current density, electrode spacing, and pH. Based on the literature, complete color and chemical oxygen demand removal can be achieved through EO treatment on real textile effluent, but requires high energy consumption, i.e., up to 500 kWh/m^3. Unless sodium sulfate (supporting electrolyte) was added into the reacting medium, only then that the energy demand could be reduced by nearly half [18]. Rai et al. reported significantly lower energy consumption values, with 20.57 kWh/m^3 for EF and 7.43 kWh/m^3 for EC. Nevertheless, these processes require additional chemical inputs and generate sludge, both of which should be taken into consideration [2].

Despite the promising capabilities of EO systems, existing research has predominantly concentrated on developing or modifying electrode materials [19–21], focusing on electrochemical interactions between the anode-cathode of a single pairing and its resulting mass transfer and degradation performance. Additionally, many studies rely on simplified reactor configurations with limited electroactive surface area, which may not represent realistic operational scales. Very few have systematically examined the kinetic behavior and energy efficiency of EO systems using multiple electrode pairings under a wide range of current densities, and none has ever reported on the mass transfer characterization within multiple electrode configurations. While applying EO treatment to real waste also provides data needed for regulatory compliance and understanding practical limitation, laboratory studies using simulated wastewater remain important because they allow researchers to control specific variables that cannot be isolated in complex tannery effluents [22]. Moreover, even when real industrial wastewater is used, it is often modified before treatment. For example, it may be filtered to remove solids that could foul electrodes, or its conductivity adjusted with salts like Na_2SO_4 or NaCl to ensure proper EO system performance [18,23].

Thus, studying synthetic tannery enables parameter optimization, allowing precise kinetic modeling of organic degradation, and detection of by-product formation.

To address these gaps, this study proposes a comprehensive assessment of EO performance on simulated high-strength tannery wastewater using both active (MMO) and non-active (BDD) anodes paired with carbonaceous (graphite) and non-carbonaceous (stainless steel) cathodes. The novelty of this work lies in its comprehensive assessment, evaluating the interplay between electrode type, enlarged effective surface area resulting from the increased number of electrode pairs, and a wide range of applied current density, not only in terms of organic pollutant degradation (using tannic acid as a model compound), but also in terms of specific energy consumption and mass transfer behavior. These insights aim to guide the selection of electrode pairings and operating conditions that achieve optimal pollutant removal with minimized energy demand, thus bridging the gap between laboratory-based studies and practical industrial applications.

2. Materials and Methods

2.1. Simulated Tannery Wastewater Preparation

Simulated tannery wastewater (STW) was prepared by dissolving 1 g/L of tannic acid ($C_{76}H_{52}O_{46}$), 2 g/L of ammonium chloride (NH_4Cl), 7 g/L of sodium chloride (NaCl), and 8 g/L of sodium sulfate (Na_2SO_4) in distilled water. All chemicals were purchased from Merck (Darmstadt, Germany), except NaCl from Chemiz (Shah Alam, Malaysia), and used without further purification. The properties of the STW in Table 1 were designed to mimic those of real tannery wastewater effluent closely [13,24], but were intentionally set higher to ensure a more stringent and conservative assessment of EO performance. Environmental characteristics of real tannery wastewater are shown in Table S1 in the Supplementary Materials.

Table 1. Properties of the simulated tannery wastewater.

Parameter	Simulated Tannery Wastewater
pH	4.29 ± 0.12
Electrical conductivity (mS/cm)	23.6 ± 0.9
Temperature (°C)	27.1 ± 0.7
Chloride, Cl^- (mg/L)	5687 ± 221
Sulfate, SO_4^{2-} (mg/L)	5415 ± 74
Ammonium, NH_4^+ (mg/L)	720 ± 33
Total Nitrogen, TN (mg/L)	503 ± 40
Total Organic Carbon, TOC (mg/L)	489 ± 77

2.2. Electrochemical System

Figure 1 depicts the electro-oxidation (EO) setup following a 2-electrode configuration. The EO was conducted in a vessel made of polyacrylic with internal dimensions of $13 \times 17 \times 13\ cm^3$. Three pairs of electrodes were arranged in parallel to one another with an interelectrode gap of 1 cm. Each electrode was connected to a direct current (DC) power supply (ATTEN, Shenzhen, China), and operated at current settings of 1, 2, and 3 A, corresponding to current densities of 2, 4, and 6 mA/cm^2, respectively. The anodes were either boron-doped diamond (BDD) (Boromond, Changsha, China) or mixed-metal oxide (MMO) (Geerwork, Baoji, China), while the cathodes were either stainless-steel (SS) (FS Metal, Melaka, Malaysia) or graphite (Yureka, Kuala Lumpur, Malaysia). The BDD was double-sided on a silicon substrate (Si/BDD), with an average coating thickness of 10–20 μm. The MMO was made of an 8:2 ruthenium-iridium coating with a thickness of 8 μm on a titanium substrate (Ti/Ru-Ir). All electrodes were $100 \times 150\ mm^2$ with 3 mm

thickness and pre-treated with 0.25 M sulfuric acid (H_2SO_4) (Merck, Darmstadt, Germany) for 30 min before usage. The total effective surface area of the electrodes submerged in electrolyte was 500 cm^2. All experiments were conducted with 2 L of the STW and replicated at least twice to ensure the reproducibility of the results.

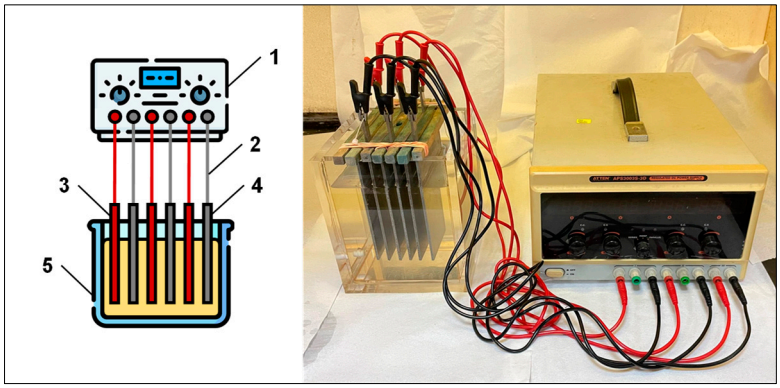


Figure 1. Experimental setup of a 2-electrode configuration (1: direct current power supply, 2: cable, 3: anode, 4: cathode, and 5: rectangular vessel).

2.3. Electrochemical Characterization

Chronopotentiometry (CP) and cyclic voltammetry (CV) were performed using the STW as electrolyte under a 3-electrode configuration, as illustrated in Figure 2. The setup involved the use of a DC power supply (Keithley 2231A-30-3) (Keithley, Solon, OH, USA) and a digital multimeter with an integrated data acquisition system (Keithley 2700 series) (Keithley, Solon, OH, USA). The DC power supply was connected to the electrode pairs, serving as the working electrode (WE) and counter electrode (CE). The multimeter was then connected to the WE and a reference electrode (RE) made of saturated silver-silver chloride ($Ag/AgCl/Cl^-$).

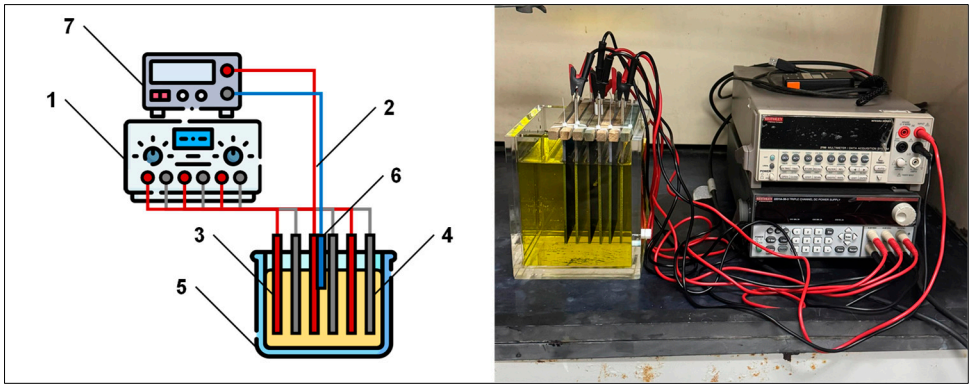


Figure 2. Experimental setup of a 3-electrode configuration (1: direct current power supply, 2: cable, 3: working electrode, 4: counter electrode, 5: rectangular vessel, 6: reference electrode, and 7: multimeter).

Mass transfer characterization experiments were performed under the same 3-electrode configuration but adopting the limiting current technique that has been widely deployed [25–27]. Experimental details can be found in Text S1 in the Supplementary Materials. Linear scan voltammetry (LSV) was then performed to reveal the limiting current plateau, which indicates the maximum oxidative current for the one-electron oxidation

reaction shown in Equation (1). The limiting current value was then used to determine the mass transfer coefficient, k_m, via Equation (2).

$$Fe(CN)_6^{4-} \rightarrow Fe(CN)_6^{3-} + e^- \quad (1)$$

$$k_m = \frac{I_{lim}}{nFAC_{lim}} \quad (2)$$

where k_m is the mass transfer coefficient (m/s), I_{lim} is the limiting current (A), n is the number of electrons corresponds to the oxidation reaction of ferrocyanide to ferricyanide, F is the Faraday constant (96,485 C/mol), A is the effective surface area of the working electrode (m^2), and C_{lim} is the molar concentration of ferrocyanide in the solution (mol/m^3).

Furthermore, the initial limiting current density (J_{lim}) of the tannery wastewater can be theoretically determined from the reaction of mineralization of tannic acid as the organic pollutant (Equation (3)) shown in Equation (4) [28,29].

$$C_xH_yO_z + (2x - z)H_2O \rightarrow xCO_2 + (2(2x - z) + y)H^+ + (2(2x - z) + y)e^- \quad (3)$$

$$J_{lim} = n_e F k_m [C_xH_yO_z] \quad (4)$$

where J_{lim} is limiting current density (A/m^2), n_e is the number of electrons corresponds to the oxidation reaction of organic compounds, [$C_xH_yO_z$] is the molar concentration of organics (tannic acid) in the solution (mol/m^3).

2.4. Water Analyses

The pH was measured using a pH meter (Mi 151) from Milwaukee, Rocky Mount, NC, USA, while conductivity and temperature were determined using a conductimeter (SevenCompact Conductivity Meter S230) by Mettler Toledo, Columbus, OH, USA. Anion and cation concentrations were analyzed using an 861 Advanced Compact Ion Chromatography (IC) system (Metrohm, Herisau, Switzerland) operated at a flow rate of 0.7 mL/min. Anion analysis was carried out using a Metrosep A Supp—150/4.0 column (Metrohm, Herisau, Switzerland), with 3.2 mM sodium carbonate and 1 mM sodium bicarbonate as the eluent and 0.01 M sulfuric acid as the regeneration solution. For cation analysis, a Metrosep C 4—150/4.0 column (Metrohm, Herisau, Switzerland) was used with an eluent containing 1.7 mM nitric acid and 0.7 mM dipicolinic acid. Prior to IC analysis, samples were filtered using a 0.2 µm regenerated cellulose (RC) membrane syringe filter (Phenomenex, Torrance, CA, USA). Total organic carbon (TOC) and total nitrogen (TN) were measured using a TOC-V CSN Total Organic Carbon Analyzer equipped with a TNM-1 Total Nitrogen Measurement unit (Shimadzu, Kyoto, Japan). TOC and TN samples were filtered through a 0.45 µm RC membrane syringe filter (Phenomenex, Torrance, CA, USA).

2.5. Kinetic Modeling

To further understand the underlying mechanism of the electro-oxidation (EO) process, the degradation kinetics of organic pollutants were analyzed using zero-order (Equation (5)), pseudo-first-order (Equation (6)), and pseudo-second-order (Equation (7)) kinetic models.

$$C = C_0 - k_0 t \quad (5)$$

$$ln\left(\frac{C}{C_0}\right) = -k_1 t \quad (6)$$

$$\frac{1}{C} = \frac{1}{C_0} + k_2 t \quad (7)$$

where C is the TOC concentration (mg/L) at t given time (min), C_0 is the initial TOC concentration (mg/L), and the rate constant are denoted as k_0 (mg/L·min) for zero-order, k_1 (/min) for pseudo-first-order, and k_2 (L/mg·min) for pseudo-second-order kinetics. To assess the accuracy of the model fitting, the root-mean-square error (RMSE) and R^2 value were calculated using Equation (S1) and Equation (S2), respectively, as shown in Text S2 in the Supplementary Materials.

2.6. Energy and Costs Calculation

The energy consumption (EC) was calculated to assess the energy efficiency of the system using Equation (8).

$$EC = \frac{E \times I \times t}{V} \quad (8)$$

where EC is the energy consumption per unit volume of treated wastewater (kWh/m^3), E is the operating voltage (V), I is the applied current (A), t is the treatment time (h), and V is the volume of treated wastewater (L).

The EC also directly relates to the overall operational cost (OC), which includes both energy usage and the cost of electrode material, and was estimated using Equation (9).

$$OC = (C_{ec} \times EC) + \left(\frac{C_{el}}{V}\right) \quad (9)$$

where OC is the operational cost per unit volume of treated wastewater (USD/m^3), C_{ec} is the unit cost of electricity (USD/kWh), C_{el} is the unit cost of the electrode material (USD), and V is the volume of treated wastewater (m^3).

3. Results and Discussion

3.1. Electrochemical Behavior Studies

The CV conducted in this study provides a better understanding of the electrochemical behavior of the reactor cell when they were equipped with three pairs of electrodes of different materials. Figure 3 illustrates the CV curves under different setups (MMO-SS, MMO-G, BDD-SS, and BDD-G).

As shown in Figure 3a, in a broader sense, BDD exhibited a wider overpotential for water electrolysis (higher overpotential for water oxidation on the anodes and higher overpotential (in cathodic (negative) sense for water reduction on cathodes). As a result, BDD effectively delayed the onset of oxygen (O_2) evolution on anodes. The commencement of the exponential form of the curve indicates the oxygen evolution reaction (OER) shown in Figure 3b, which begins at 1.325, 1.437, 2.571, and 3.273 V/V_{SHE} for MMO-G, MMO-SS, BDD-G, and BDD-SS, respectively. It is also evident that the BDD-SS pairing provides the widest anodic potential window, allowing more room for organic oxidation before oxygen evolution begins.

The commencement of the hydrogen evolution reaction (HER) can be seen in Figure 3c. The plot shows that at very low currents (less than −0.5 A), hydroxide ion (OH^-) and hydrogen (H_2) were already generated. Among the electrode pairings, each cathode exhibits a distinctly different cathodic overpotential. MMO paired with the cathodes exhibits higher potentials (closer to 0 V), while BDD paired with the same cathodes shows lower, more negative potentials, resulting in a wider cathodic potential window. Consequently, greater OH^- generation and H_2 evolution are expected on SS and graphite when paired with BDD compared to when they are paired with MMO. However, these OH^- and H_2 activities have minimal influence on the degradation of organic materials.

Figure 4 depicts the value of anode and cathode potentials for different electrode pairings from CP measurements when they were subjected to an applied current of

1, 2, and 3 A (2, 4, and 6 mA/cm^2). The values are also tabulated in Table S2 in the Supplementary Materials.

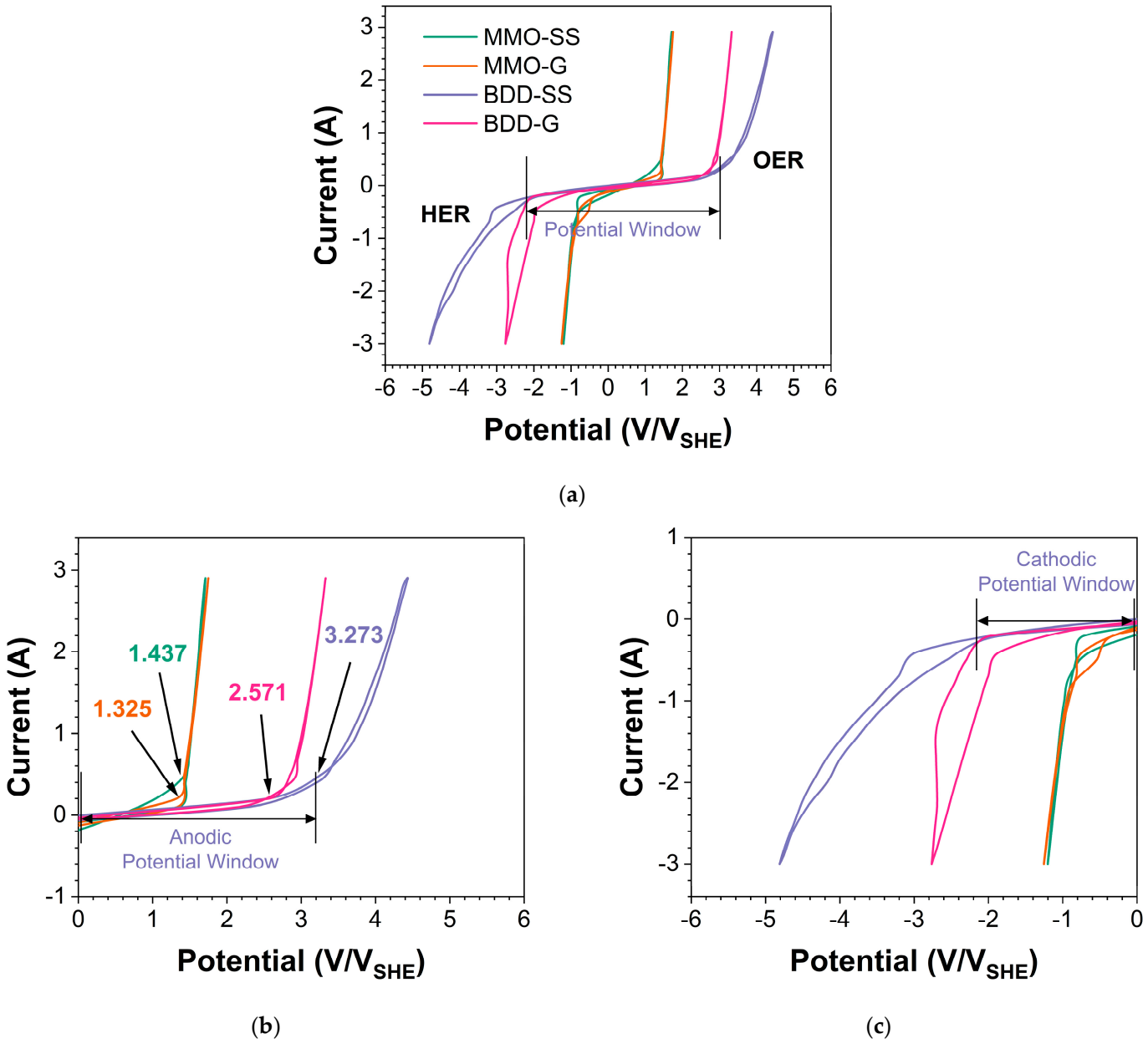


Figure 3. Cyclic voltammetry measurements of: (**a**) The simulated tannery wastewater; (**b**) Anodic regions; and (**c**) Cathodic regions of different electrode pairings.

CP results in Figure 4 revealed the lowest and highest electrode potentials for each electrode pairing: −0.923 and 1.732 V/V$_{SHE}$ for MMO-SS, −2.267 and 1.761 V/V$_{SHE}$ for MMO-G, −1.489 and 4.334 V/V$_{SHE}$ for BDD-SS, and −1.546 and 3.342 V/V$_{SHE}$ for BDD-G. These values indicate that the anode potentials of MMO-based pairings remained below the standard redox potential required for hydroxyl radical formation (+2.8 V/V$_{SHE}$), suggesting that hydroxyl radical generation was unlikely across all applied current densities for these configurations. In contrast, both BDD-based pairings reached and exceeded this threshold, confirming the feasibility of hydroxyl radical formation throughout the tested conditions. Furthermore, potential ranges associated with other redox reactions expected to occur in each electrode pairing are illustrated in Figure 5.

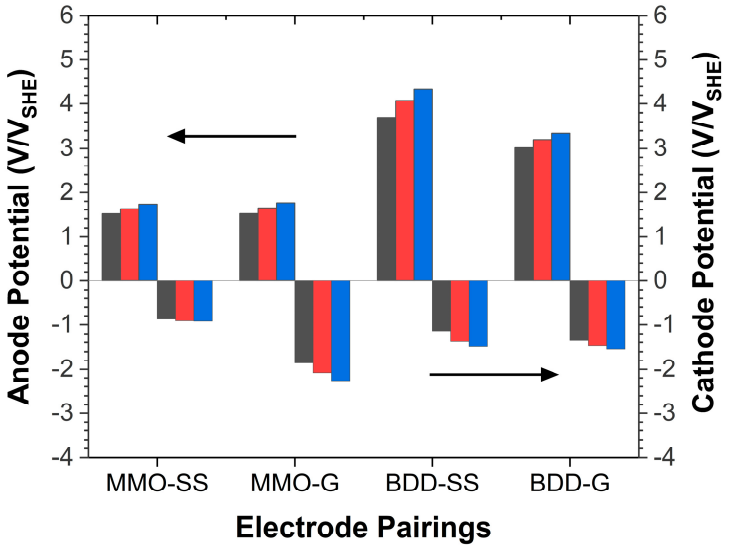


Figure 4. Chronopotentiometry measurements to obtain electrode potential (■: 2 mA/cm^2, ■: 4 mA/cm^2, ■: 6 mA/cm^2).

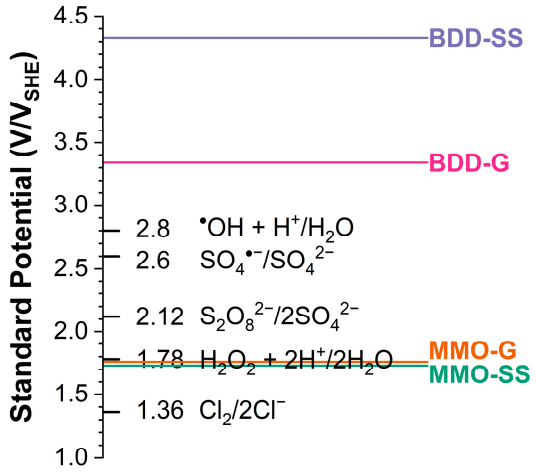


Figure 5. Standard redox potentials for different electrode pairings.

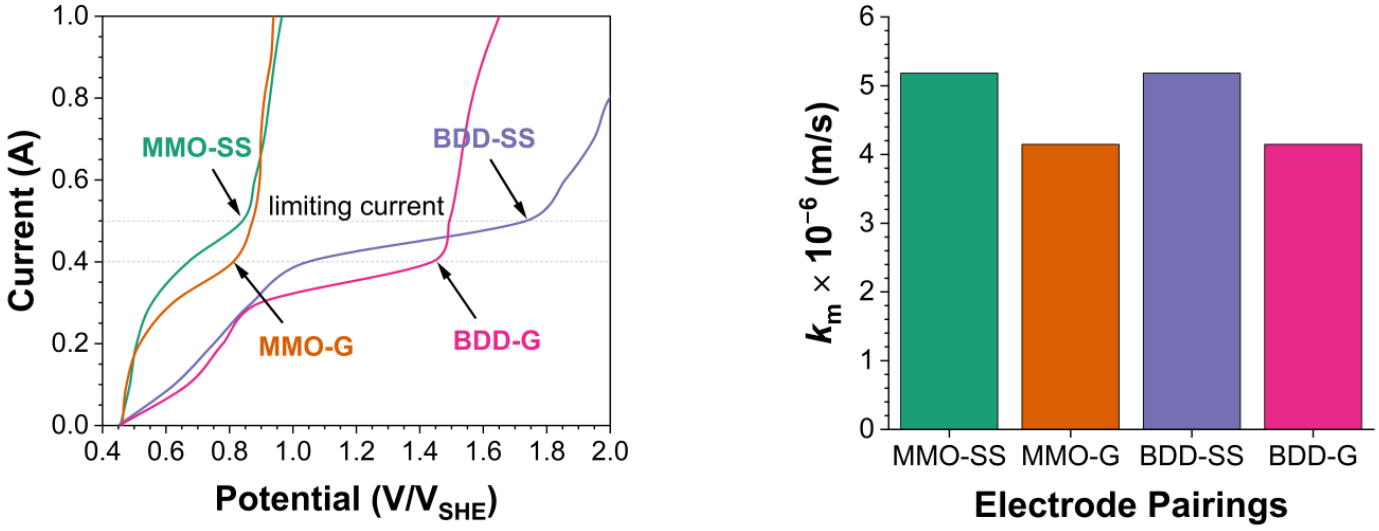
As seen in Figure 5, BDD-SS and BDD-G electrodes are capable of generating additional oxidants such as sulfate radicals ($SO_4^{\bullet-}$), persulfate ($S_2O_8^{2-}$), hydrogen peroxide (H_2O_2), and active chlorine (Cl_2), in addition to hydroxyl radicals (•OH). In contrast, MMO-G and MMO-SS predominantly produce chlorine-based oxidants, as their anode potentials are insufficient to initiate the formation of other species. These observations offer valuable insight into the types of radical reactions likely occurring in each system. These insights play a vital role in system performance and how the degradation mechanism works.

3.2. Mass Transfer Characterization

Figure 6a depicts the LSVs of the electrochemical reactor when it was equipped with three pairs of different electrode materials (MMO-SS, MMO-G, BDD-SS, and BDD-G). I_{lim} for different electrode pairings were measured from the plotted LSVs, and their values are tabulated in Table S3 in the Supplementary Materials. Notably, comparable I_{lim} values were observed for the MMO-SS and BDD-SS pairings, as well as for MMO-G and BDD-G, indicating a similarity in the current that limits the process.

Referring to the values of the I_{lim}, k_m was calculated using Equation (2) and their values are presented in Figure 6b. The calculated k_m values were 5.18 × 10^{-6} m/s for MMO-SS and BDD-SS, and 4.15 × 10^{-6} m/s for MMO-G and BDD-G. This range of

values falls within those reported in the literature; 1.7 to 5.9 × 10^{-6} m/s for a stirred tank reactor [30,31]. No remarkable improvement was noticed with respect to the k_m under this investigated parallel plate setup, despite being in multielectrode mode, other than only the increase in effective surface area. It was also found that using SS as cathodes would offer a better k_m than for graphite cathode. The reason could be because both SS and graphite were planar in this work. Our results suggested that the electrical conductivity of the metallic SS outweighed the porous feature of the graphite, which manifested in better k_m for the former.



(**a**) (**b**)

Figure 6. Plot of: (**a**) Experimental I_{lim} curves; and (**b**) Calculated k_m as a function of different electrode pairings.

Using the determined k_m, the J_{lim} during the electro-oxidation of the STW was evaluated using Equation (4). The J_{lim} was determined to be 7.76 mA/cm^2 for MMO-SS and BDD-SS, and 6.21 mA/cm^2 for MMO-G and BDD-G. The applied current density (J_{app}) in this work ranged from 2 to 6 mA/cm^2. It means that, initially, the degradation process will be controlled by charge-transfer regime because instantaneous J_{lim} is higher than J_{app}. As the time evolves, the pollutants decreases and the corresponding J_{lim} will be less than J_{app}, the abatement process would shift from a current control regime to a mass-transfer limited process [32].

3.3. Role of Current Density

Figure 7 illustrates the degradation of TOC over 8 h of treatment at varying current densities using different electrode materials.

As the applied current density increased from 2 to 4 mA/cm^2, the degradation efficiency also improved, attributed to the enhanced generation of oxidizing species and increased electron transfer at the anode surface [18]. However, further increasing the current to 6 mA/cm^2 resulted in a decrease in degradation efficiency. The MMO-SS and MMO-G configurations achieved their highest TOC removal efficiencies at 4 mA/cm^2, reaching 60.52 ± 0.02% and 63.85 ± 0.02%, respectively. Similarly, the BDD-SS and BDD-G pairings also achieved their highest TOC removals at 4 mA/cm^2, with 98.01 ± 0.03% and 89.48 ± 0.03%, respectively. These results indicate that the performance at 4 mA/cm^2 exceeded that at 6 mA/cm^2, likely due to the increased occurrence of side reactions at higher current densities, particularly toward the end of the treatment period.

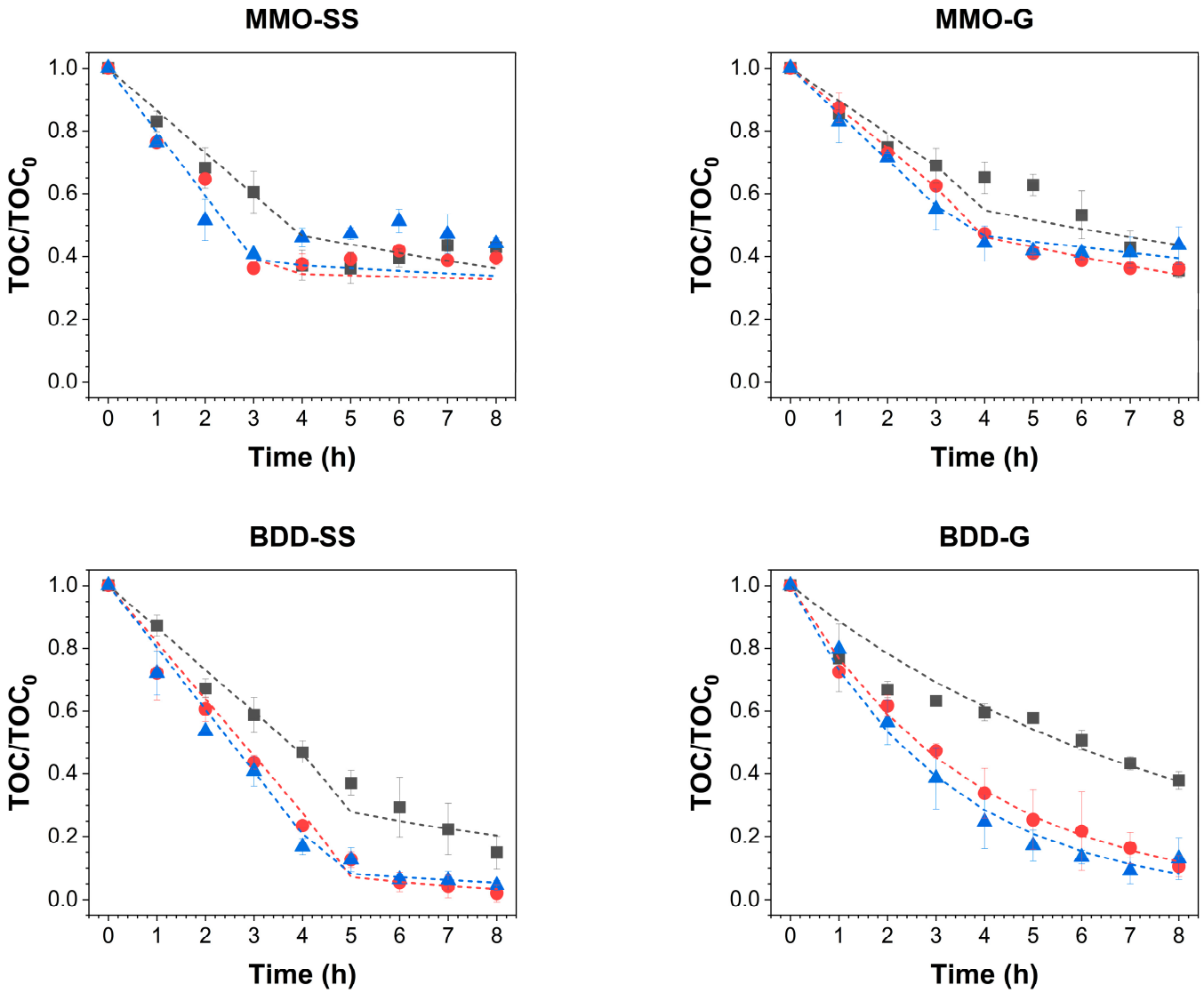


Figure 7. Influence of applied current densities on TOC degradation (■, ·····: 2 mA/cm^2; ●, ·····: 4 mA/cm^2; ▲, ·····: 6 mA/cm^2) for different electrode pairings. The scatter plots represent the experimental data, while the dotted lines indicate the theoretical model curves.

It is also evident that, beyond a certain point, EO utilizing MMO as anodes exhibits a plateau in degradation performance, indicating the attainment of maximum removal efficiency. The EO systems employing BDD electrodes exhibited a similar trend, showing a transition from a linear decrease to an exponential decay in TOC removal. These experimental results are consistent with findings reported in previous studies [16,33]. This can be attributed to the mass transfer limitation, where the reaction rate becomes faster than the rate at which the pollutants can reach the electrode surface [34]. Under such conditions, excess oxidants may react with each other or with other competing species, such as oxygen, rather than with the target pollutants. Another possible reason is the increased dominance of the oxygen evolution reaction (OER) at higher current densities after approximately 3 to 4 h of operation [35]. In chloride-containing solutions, such as this simulated tannery wastewater, chlorine evolution reaction (CER) may also occur at the anode, where the presence of chloride leads to the formation of various reactive chlorine species (RCS) [36]. The formation of RCS, such as chlorine gas (Cl_2), hypochlorous acid (HClO), and hypochlorite ion (ClO^-), involves the abatement of chloride in this simulated tannery wastewater [37,38]. Figure 8 illustrates the removal of chloride ion over time during 8 h of treatment.

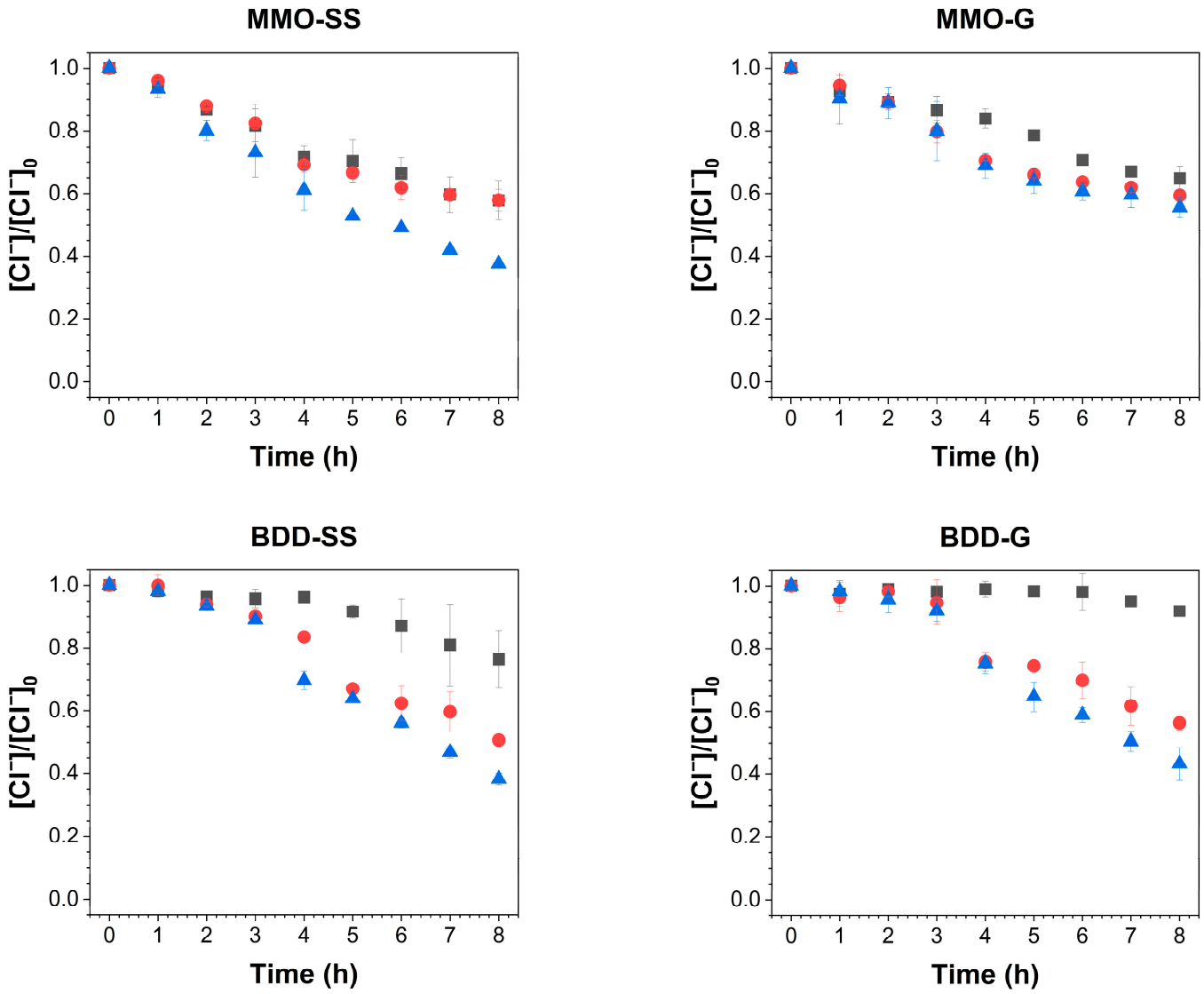


Figure 8. Chloride degradation for different applied current densities (■: 2 mA/cm^2, ●: 4 mA/cm^2, ▲: 6 mA/cm^2) using different electrode pairings.

As shown, the highest applied current density (6 mA/cm^2) resulted in improved chloride removal rates, achieving 62.45 ± 0.01% for MMO-SS, 44.37 ± 0.03% for MMO-G, 61.90 ± 0.02% for BDD-SS, and 56.78 ± 0.05% for BDD-G. While BDD-based configurations demonstrated strong chloride removal, the MMO-SS pairing exhibited the highest chloride elimination, suggesting greater formation of RCS. Although RCS are also potent oxidants, they are known to exhibit lower reactivity and higher selectivity compared to hydroxyl radicals [39]. This characteristic may explain why BDD-based systems achieved higher organic degradation performance despite forming less RCS. The relevant reactions are presented in Equations (10)–(12).

$$2Cl^- \rightarrow Cl_2 + 2e^- \quad (10)$$

$$Cl_2 + H_2O \rightarrow HClO + H^+ + Cl^- \quad (11)$$

$$HClO \rightarrow H^+ + ClO^- \quad (12)$$

Other than chloride, ammonium was also examined. Figure 9 illustrates the degradation of ammonium in the EO system for different electrode pairings under various current densities.

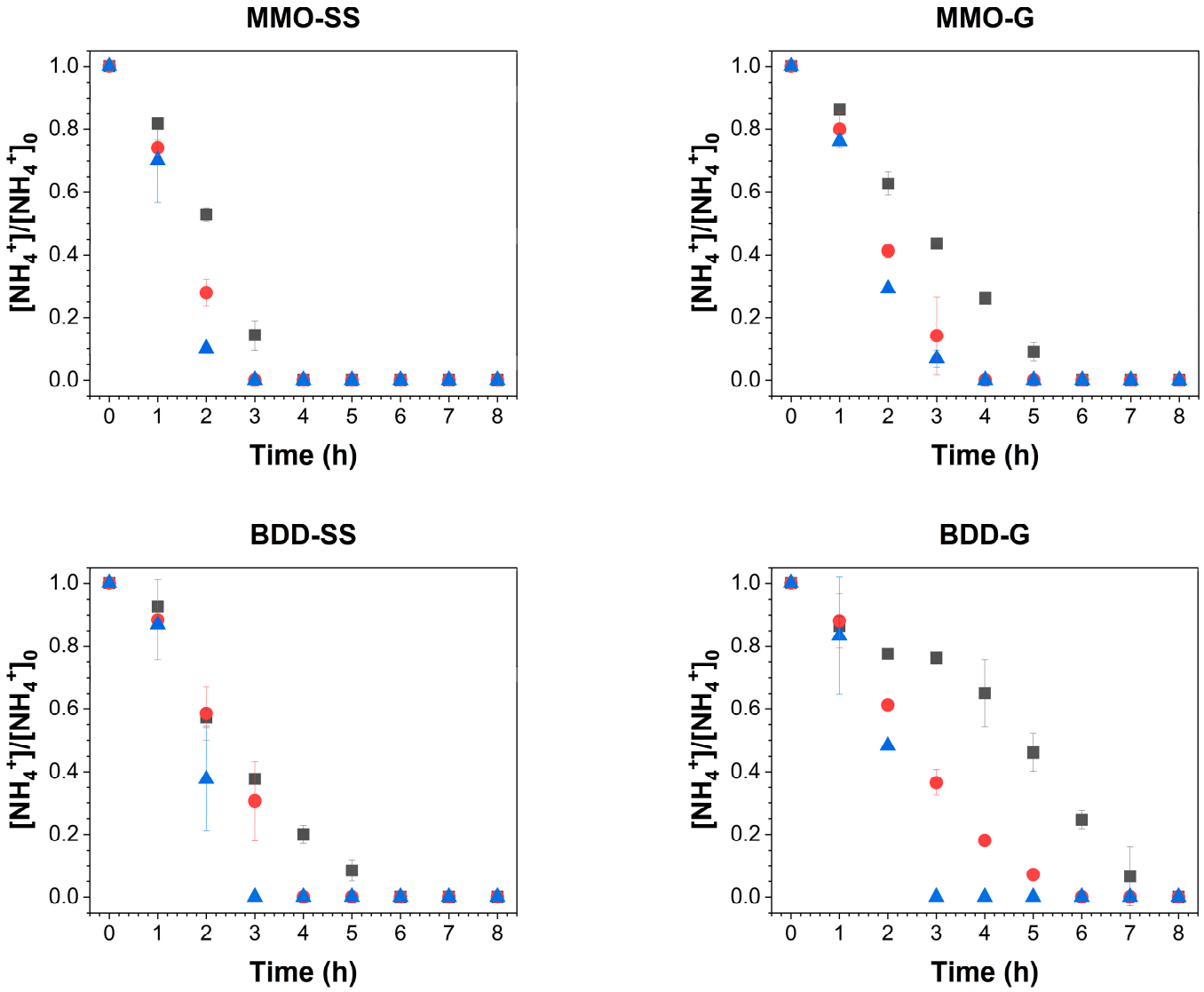


Figure 9. Ammonium degradation for different applied current densities (■: 2 mA/cm^2, ●: 4 mA/cm^2, ▲: 6 mA/cm^2) using different electrode pairings.

The results show that complete ammonium removal was achieved across all current densities and electrode configurations after 8 h of treatment. Among the pairings, MMO-SS demonstrated the fastest degradation, achieving complete removal within the first 3 to 4 h, followed by MMO-G and BDD-SS, which reached full removal within 4 to 5 h. The BDD-G configuration exhibited the slowest performance, requiring up to 7 h for complete ammonium degradation.

The complete abatement of ammonium is likely due to the dissociation of ammonium chloride into ammonium (NH_4^+) and chloride (Cl^-) ions at neutral pH. The ammonium ions are then oxidized at the anode, leading to the formation of nitrite (NO_2^-) and/or nitrate (NO_3^-), depending on the reaction conditions [40]. The relevant oxidation reactions are as Equations (13)–(15):

$$NH_4^+ \rightarrow NH_3 + H^+ \quad (13)$$

$$NH_3 + 2H_2O \rightarrow NO_2^- + 7H^+ + 6e^- \quad (14)$$

$$NH_3 + 3H_2O \rightarrow NO_3^- + 9H^+ + 8e^- \quad (15)$$

In the presence of chloride ions, an indirect oxidation may contribute to the degradation of ammonium, as it reacts with the generation of HClO [41]. This can lead to the production of either nitrogen gas (N_2) or NO_3^- in the following Equations (16) and (17):

$$2NH_4^+ + 3HClO \rightarrow N_2 + 3H_2O + 5H^+ + 3Cl^- \quad (16)$$

$$NH_4^+ + 4HClO \rightarrow NO_3^- + H_2O + 6H^+ + 4Cl^- \quad (17)$$

Depending on the pH of the solution, the type of nitrogen compounds present in a solution vary. In acidic solutions, N_2 predominates. Conversely, in alkaline solutions, there is a significant presence of NO_3^- because it is less suitable for reduction at the cathode.

Accordingly, it is important to emphasize that in scenarios where the formation of hydroxyl radicals (•OH) is anticipated, particularly in systems using BDD anodes, secondary reactions involving NH_4^+ may also occur through a series of chain reactions with •OH [42]. These secondary reactions forming various nitrogenous species, as shown in Equations (18)–(20) [43,44]. Subsequently, the in situ generated oxidant HClO may react with NH_4^+ to form aminochlorides (commonly known as chloramines, such as monochloramine (NH_2Cl), dichloramine ($NHCl_2$), and trichloramine (NCl_3)) through the following reactions (Equations (21)–(23)). Although these secondary reactions also produce reactive species, their oxidative potential and ability to break organic bonds are generally lower than that of •OH.

$$NH_4^+ + \bullet OH + 3H_2O \leftrightarrow NO_3^- + 10H^+ + 8e^- \quad (18)$$

$$NO_2^- + \bullet OH + H_2O \leftrightarrow NO_3^- + 2H^+ + 2e^- \quad (19)$$

$$NH_4^+ + 3\bullet OH + OH^- \leftrightarrow \frac{1}{2}N_2 + 4H_2O + 3e^- \quad (20)$$

$$NH_4^+ + HClO \rightarrow NH_2Cl + H_2O + H^+ \quad (21)$$

$$NH_2Cl + HClO \rightarrow NHCl_2 + H_2O \quad (22)$$

$$NHCl_2 + HClO \rightarrow NCl_3 + H_2O \quad (23)$$

Similarly, due to the high Cl^- concentrations in the STW, it is likely to react with •OH, forming reactive species such as hypochlorite (ClO^-), chlorite (ClO_2^-), chlorate (ClO_3^-), and perchlorate (ClO_4^-) ions as seen in Equations (24)–(27) [44,45]. All of those reactive species unfortunately are considered toxic and persistent [46].

$$Cl^- + \bullet OH \rightarrow ClO^- + HClO \quad (24)$$

$$ClO^- + \bullet OH \rightarrow ClO_2^- + H^+ + e^- \quad (25)$$

$$ClO_2^- + \bullet OH \rightarrow ClO_3^- + H^+ + e^- \quad (26)$$

$$ClO_3^- + \bullet OH \rightarrow ClO_4^- + H^+ + e^- \quad (27)$$

Additionally, the active chlorine species produced (Cl_2, HClO, and ClO^-), as previously discussed, act only as intermediates and are quickly converted into either chlorate, perchlorate, or other species [44]. This study tested the chlorate and perchlorate generation in optimum configuration (BDD-SS pair operated at 4 mA/cm^2) and provided in Figure 10 below.

The results indicate that both chlorate and perchlorate concentrations increased progressively over the 8 h reaction period, reaching final concentrations of approximately

1674.82 mg/L (chlorate) and 45.20 mg/L (perchlorate). According to the literature, when dimensionally stable anodes (DSA) such as MMO are used, ClO_3^- typically becomes the dominant oxidation intermediate, while ClO_4^- formation remains negligible due to the limited generation of •OH radicals. In contrast, BDD anodes are known to favor the formation of ClO_4^- during prolonged electrolysis because of their high •OH production capacity [47–49]. However, in the present study, ClO_3^- formation was approximately 37 times higher than ClO_4^- despite the use of BDD. This behavior may be attributed to two factors. First, the rate-limiting step in ClO_4^- formation involves the direct electron transfer of ClO_3^- on the BDD surface to form the $ClO_3^•$ radical, which subsequently reacts with •OH to yield $HClO_4$ [47]. Under high Cl^- concentrations, Cl^- can outcompete ClO_3^- for oxidation at the anode surface, suppressing ClO_4^- formation. Second, the extremely short lifetime of •OH radicals prevent them from reaching the bulk solution, meaning that ClO_4^- formation is restricted to the anode surface [50].

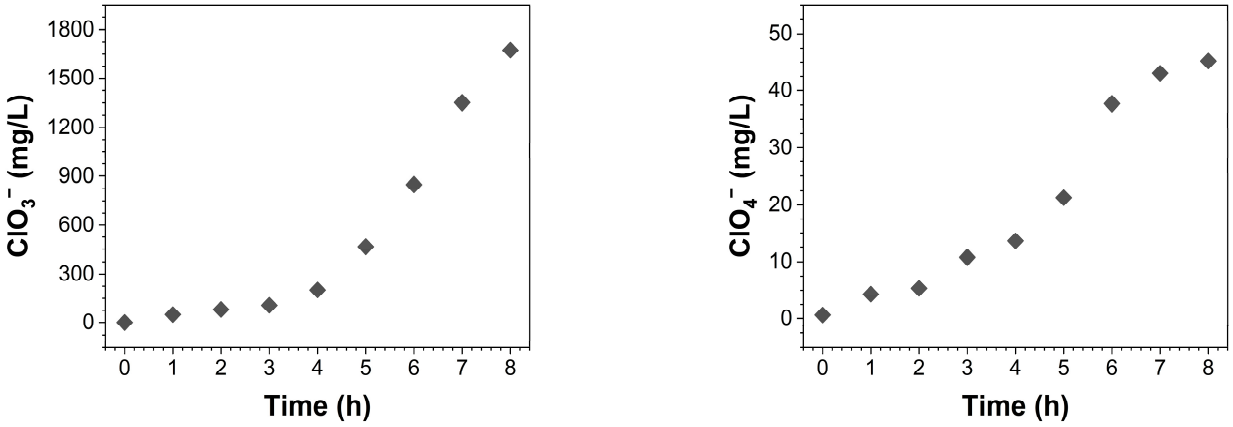


Figure 10. Chlorate and perchlorate formation in electro-oxidation using BDD-SS pair.

To summarize, the simulated tannery wastewater contained very high concentrations: TOC ~489 mg/L, chloride ~5687 mg/L, sulfate ~5415 mg/L, and ammonium ~720 mg/L. In our experiments, the BDD-SS configuration operating at 4 mA/cm^2 proved the most effective and energy-efficient: achieving ~98% TOC removal (with a final concentration of 12.44 mg/L), ~49% chloride removal (with a final concentration of 3158 mg/L), and 100% ammonium removal, while sulfate levels remained essentially unchanged. As of the date of this publication, under the Environmental Quality (Industrial Effluent) Regulations 2009 (under Environmental Quality Act 1974, Malaysia), there are no fixed discharge concentration limits for TOC, chloride, or sulfate under the Fifth Schedule, "Acceptable Conditions for Discharge of Industrial Effluent or Mixed Effluent of Standards A and B" [51]. These parameters fall under "List of Parameters for Discharge of Industrial Effluent or Mixed Effluent which Best Management Practice to be adopted" requirements of the Ninth Schedule, which means a case where a practical approach is needed to minimize environmental impacts, rather than a strict numeric limit.

3.4. Role of Electrode Pairing

To further evaluate the influence of electrode materials on the electro-oxidation process of tannery wastewater, a comparative analysis was conducted using various anode-cathode pairings. Figure 11 presents the TOC degradation profiles at current densities of 2, 4, and 6 mA/cm^2, respectively. At the lowest current density, as shown in Figure 11a, all electrode combinations exhibited a declining TOC trend except for MMO-SS, which attained a plateau after 4 h with a maximum removal efficiency of 62.85 ± 0.05%. Among all configurations,

BDD-SS achieved the highest TOC removal of 85.15 ± 0.05% after 8 h, followed by MMO-G (64.40 ± 0.03%) and BDD-G (62.17 ± 0.03%).

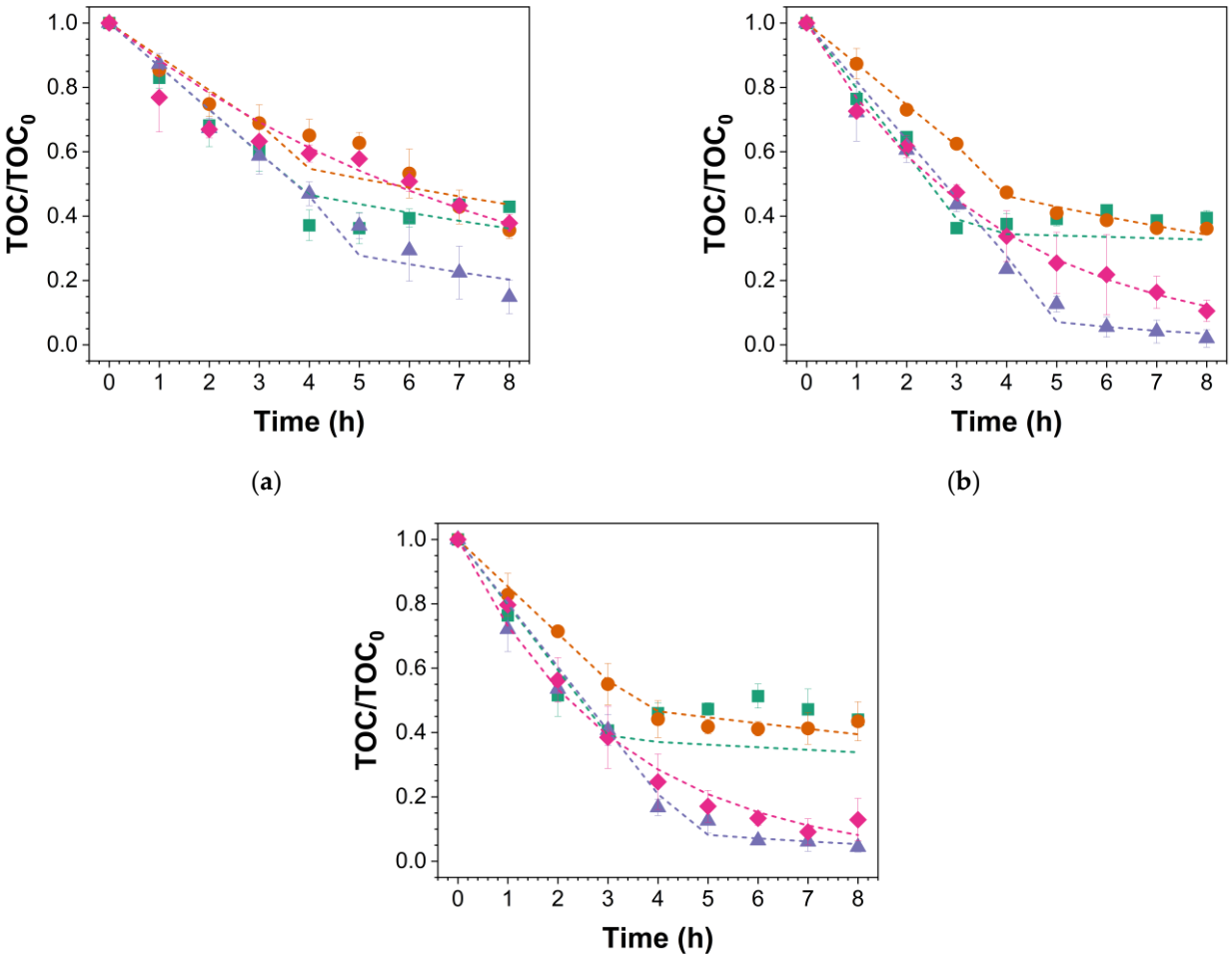


Figure 11. Influence of electrode pairings on TOC degradation at (**a**) 2, (**b**) 4, and (**c**) 6 mA/cm^2 (■: MMO-SS, ●: MMO-G, ▲: BDD-SS, ◆: BDD-G). The scatter plots represent the experimental data, while the dotted lines indicate the theoretical model curves.

A similar trend is observed in Figure 11b,c, where the maximum TOC removal by the MMO-SS pairing occurs one hour earlier, reaching its peak after 3 h of treatment. Despite this, BDD-SS consistently achieved the highest removal efficiencies after 8 h, while MMO-SS showed the lowest performance. Specifically, at 4 mA/cm^2 (Figure 11b), BDD-SS achieved a TOC removal of 98.01 ± 0.03%, whereas MMO-SS reached only 60.52 ± 0.02%. At 6 mA/cm^2 (Figure 11c), BDD-SS maintained a high removal rate of 95.57 ± 0.02%, compared to 55.96 ± 0.02% for MMO-SS. The degradation curves clearly indicate that BDD-based electrode pairings offer more favorable outcomes for organic pollutant removal than MMO pairings.

This difference can be attributed to the nature of the anode materials, which are classified as active or non-active (passive). Active anodes like MMO tend to follow more selective oxidation pathways, where the direct oxidation of organics competes with the OER. Moreover, the •OH formed may be further oxidized into higher oxides that exhibit selective behavior and decompose into oxygen. In contrast, non-active anodes like BDD promote non-selective oxidation, capable of direct oxidation of organics on the electrode surface and generate hydroxyl radicals that enable indirect oxidation in the bulk solution [14,52].

Comparing those two types of anodes, there have been a variety of reports on the lifespan of BDDs, depending on the quality and the method of fabrication by the supplier, applied conditions, and the properties of the effluent to be treated. From the literature, the BDD can last for 10 years and even longer [23,53]. Meanwhile, MMO electrodes generally have shorter lifetimes and lower electrochemical stability. For instance, MMO deactivation due to passivating hydroxide layer formation has been reported to occur after only 4 h of electrolysis in some studies [14] and other reports after 195 h [13], although this can vary depending on MMO composition. The service life of MMO can be extended by incorporating noble metals such as iridium or ruthenium in the outer layer, which is more resistant to corrosion.

Regarding the influence of cathode materials, the cathode generally plays a limited role in organic degradation in electro-oxidation processes because mineralization primarily depends on anodic radical production, it becomes more significant in systems such as electro-Fenton, where continuous hydrogen peroxide generation is required [54]. Nevertheless, Figure 11 suggested that stainless steel performs slightly better than graphite when paired with BDD anodes. This is consistent with our finding on the value of k_m for different electrode pairings discussed before, where the improvement is likely due to the higher electrical conductivity of SS, which ranges from 1.33 to 1.45 $\times$ 10^6 S/m, compared to that of graphite, which ranges from 1.27 to 3.00 $\times$ 10^5 S/m [55,56]. However, the CV measurements in the cathodic region also showed no noticeable differences between the cathodes paired with MMO, and only the BDD-SS configuration exhibited a wider potential window than BDD-G. This indicates that although the cathode materials differ in conductivity, the effect is minimal, and the anode largely governs the organic removal performance.

Furthermore, as previously discussed based on CV measurements of different electrode pairings, oxygen evolution occurs at the anodes and hydrogen evolution occurs at the cathodes at electrode-dependent potentials. This confirms that once required potentials are reached, both the OER and HER occur. Since the STW used in this study is acidic, the corresponding reactions can be expressed as:

$$2H_2O \rightarrow O_2 + 4H^+ + 4e^- \quad (28)$$

$$2H^+ + 2e^- \rightarrow H_2 \quad (29)$$

In terms of the reductive activities on cathode, unlike in electro-Fenton processes where HER competes with oxygen reduction to produce H_2O_2, therefore reducing the treatment efficacy [2], the limited availability of dissolved oxygen on cathode favors HER over the oxygen reduction reaction (ORR). It means that cathodic reactions do not directly contribute to organic degradation. There could have been a participation of atomic hydrogen (H*) in the dechlorination of organic pollutants if the pollutants bear halogenic compound, as reported by Wei at al. [57]. The H* could contribute to the degradation of chlorinated organic intermediates.

On anode, there have been some reports on the competition between OER with organic oxidation when high applied current densities were applied [58]. The concurrence was marked with MMO anodes, where the standard electrode potential of oxygen evolution and chlorine evolution reactions were close [36]. Nonetheless with BDD anodes, the production of hydroxyl radicals is still predominant. Furthermore, according to Wei et al., the O_2 produced at the anode could serve as a precursor for the production of reactive oxygen species (ROS) [57].

3.5. Kinetic Modeling of Pollutant Removal

Kinetic modeling is commonly applied in wastewater treatment to better understand, predict, and optimize the efficiency of pollutant removal. In this study, various kinetic models were employed: pseudo-first-order, pseudo-second-order, and a sequence of zero-order and pseudo-first-order to identify the best-fitting kinetic model to our experimental data. Table S4 in Supplementary Materials presents the corresponding kinetic constants along with their evaluated RMSE values (Equation (S1)) complemented by the calculated R^2 regression value (Equation (S2)).

The analysis revealed that for most electrode pairings (MMO-SS, MMO-G, and BDD-SS), the mixed zero-order and pseudo-first-order model provided the best fit, as evidenced by the lowest RMSE values compared to other kinetic models. At a current density of 4 mA/cm^2, the lowest RMSE values were 21 (R^2 = 0.945) for MMO-SS, 5 (R^2 = 0.997) for MMO-G, and 25 (R^2 = 0.981) for BDD-SS. These results demonstrate a good mathematical fitting between experimental and theoretical data, further supported by R^2 values approaching 1. The exception was BDD-G, which showed the best fit with the pseudo-first-order model, yielding the lowest RMSE of 12 and the highest R^2 value (0.995) at the same current density. Although RMSE values exceeded 1, normalization by the mean experimental value resulted in an error of less than 10%, which is generally considered acceptable. These findings suggest that the electro-oxidation process in systems with multiple electrode pairings tends to transition from a charge-transfer-controlled (zero-order) regime to a mass-transfer-controlled (pseudo-first-order) regime over time. Consistent with this observation, Bravo-Yumi et al. reported that the kinetics of complex substrates may follow mixed-order behavior, typically exhibiting an initial linear degradation phase followed by a nonlinear trend as the reaction progresses [23].

The fitted results in Table S4 (also plotted in Figure 7) further showed that in terms of electrode material, BDD-based configurations consistently exhibited higher kinetic rate constants than those with MMO. For instance, the k_0 values for BDD-SS were 1.245, 1.660, and 1.915 mg/L·min at 2, 4, and 6 mA/cm^2, respectively, compared to 0.991, 1.433, and 1.407 mg/L·min for MMO-SS. This difference in kinetic rates indicates the higher oxidizing capability of BDD with respect to the MMO, whereby the abatement of organics occurs both heterogeneously and homogeneously in the former, further assisted by electrogenerated radical species in the bulk solution, thereby achieving higher overall degradation rates [37,52]. In contrast, due to the absence of •OH in the MMO system, the degradative pathway was via a direct electron transfer on MMO surfaces, plus the homogeneous oxidation reactions in the bulk, thanks to the formation of reactive chlorinated and oxygenated species.

3.6. Energy and Costs Consumption

Energy consumption (EC) is a critical factor, particularly for industrial applications, as it directly influences the overall efficiency and economic feasibility of electrochemical treatment processes. Identifying the optimal current density is essential to balance effective pollutant degradation with minimal energy demand. Figure 12 illustrates the recorded energy consumption for various electrode pairings operated at three different current densities over an 8 h treatment period.

Based on the calculations, applying lower current densities led to reduced energy consumption, as less electrical power was required within the electrochemical system. The EC, measured from highest to lowest current densities, was found to be 51, 27.40 ± 0.85, and 11.9 ± 0.14 kWh/m^3 for MMO-SS; 54 ± 4.24, 30, and 12.9 ± 0.42 kWh/m^3 for MMO-G; 99.3 ± 14.85, 84.6 ± 5.94, and 31.1 ± 13.72 kWh/m^3 for BDD-SS; and 97.5 ± 0.42, 69.4 ± 0.85, and 34.8 ± 15.84 kWh/m^3 for BDD-G, respectively. Considering the degra-

dation performance discussed in the previous section, the optimal EC was observed at a current density of 4 mA/cm^2.

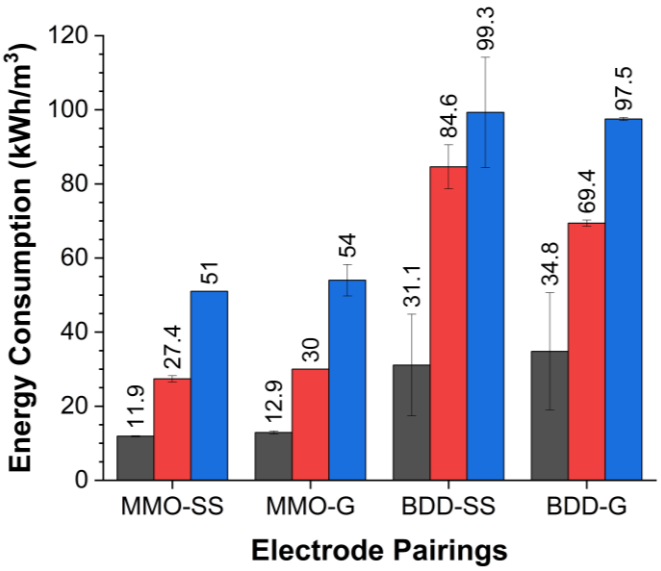


Figure 12. Energy consumption at different applied current densities for all pairings (■: 2 mA/cm^2, ■: 4 mA/cm^2, ■: 6 mA/cm^2).

A comparison between electrode pairings revealed that BDD-based configurations consumed nearly two times more energy than MMO-based ones. This can be attributed to the inherent characteristics of MMO anodes, which primarily support direct oxidation mechanisms that operate at lower cell voltages, thereby reducing energy demand [59]. In contrast, BDD anodes promote both direct and indirect oxidation, which typically require higher applied voltages, thus increasing energy consumption relative to MMO systems [52].

A review of the literature indicates that the energy demand reported in our study is consistent with previously published EO systems treating tannery wastewater. One relevant study on simulated tannery wastewater reported an energy requirement ranging from 104 to 2547 kWh/kg TOC, depending on the anode material used, under an applied current density of 25 mA/cm^2 for 4 h of treatment [14]. In comparison, when the specific energy consumption in our study was calculated at an operating current density of 4 mA/cm^2, values of 106.93 ± 0.80 kWh/kg TOC for MMO-SS, 115.46 ± 4.45 kWh/kg TOC for MMO-G, 137.04 ± 3.31 kWh/kg TOC for BDD-G, and 160.78 ± 39.11 kWh/kg TOC for BDD-SS were obtained. These energy demands are slightly higher but remain within the reported range, likely due to the lower applied current density and longer treatment time used in our work. It should also be highlighted that the previous study employed a single-pair electrode configuration, whereas our system used three electrode pairs, which naturally increases total energy consumption. Furthermore, our study treated a higher-strength tannic acid solution (1000 mg/L), which is approximately 13 times higher than the initial total phenol concentration (73.2 mg/L) reported in the literature. Since specific energy consumption is normalized per kilogram of TOC removed, higher pollutant loads generally result in lower specific energy values, reflecting more efficient energy use relative to the amount of degraded organic matter. Additionally, although the energy demand is relatively high, EO is not generally intended to replace low-cost bulk-treatment processes. Instead, it functions as a polishing or finishing step for recalcitrant contaminants, where higher energy intensity is acceptable due to the smaller treated volume.

These findings suggest that for industrial applications where energy efficiency is critical and the pollutant concentration is not excessively high, MMO-based pairings may

offer a more cost-effective solution. Between the two MMO combinations, MMO-SS and MMO-G exhibited comparable energy consumption; however, MMO-SS achieved notably higher pollutant removal efficiency, making it the more favorable option.

Conversely, for the treatment of high-strength, recalcitrant wastewater such as tannery effluent, and in cases where budget constraints are less limiting, investing in BDD-based systems may be advantageous for long-term use. BDD electrodes not only deliver superior degradation performance but also possess excellent corrosion resistance due to their diamond coating. Among all configurations, the BDD-SS pairing operated at 4 mA/cm^2 emerged as the most effective and energy-efficient setup under the tested conditions.

However, the cost of electrode materials also remains a significant consideration, with BDD being considerably more expensive than MMO. The electrode prices were 30 USD/piece for MMO, 400 USD/piece for BDD, 30 USD/piece for stainless steel, and 60 USD/piece for graphite, while the electricity tariff in Malaysia was RM 0.22/kWh (equivalent to 0.052 USD/kWh as of July 2025). Using Equation (9), Table 2 presents the operational costs (OC) in this study, excluded maintenance, sludge treatment, and chemical consumption, as the electro-oxidation process did not involve external chemical additives and generated no sludge [23].

Table 2. Operational costs of different electrode pairings with optimum current density.

Electrode Pairings	Tariff Costs (USD/m^3)	Anode Costs (USD/m^3)	Cathode Costs (USD/m^3)	Total Operational Costs (USD/m^3)
MMO-SS	1.42	45	45	91.42
MMO-G	1.56	45	90	136.56
BDD-SS	4.40	600	45	649.40
BDD-G	3.61	600	90	693.61

The total operational costs of EO systems using BDD pairings were substantially higher than those with MMO, as expected. It should also be noted that electrode costs may vary depending on the supplier. Another supplier offers BDD and graphite electrodes with similar properties at lower prices, approximately 165 USD/piece (Worldia, Beijing, China) for BDD and 5.2 USD/piece (Yuantai, Pingdingshan, China) for graphite. A comparison between the costs of the current electrodes and their alternatives is presented in Table 3.

Table 3. Estimated costs of current and alternative electrode materials used in electro-oxidation.

Electrode Pairings	Current OC (USD/m^3)	Alternative OC (USD/m^3)
MMO-SS	91.42	91.42
MMO-G	136.56	54.36
BDD-SS	649.40	296.90
BDD-G	693.61	258.91

4. Conclusions

This study demonstrated that the degradation efficiency of simulated tannery wastewater in multi-pair EO systems is significantly influenced by both current density and electrode material. The BDD-based configurations, particularly BDD-SS operated at 4 mA/cm^2, exhibited the highest TOC removal efficiency (98%), demonstrating higher efficiency than MMO-based systems. Although energy consumption increased with higher current densities, the results revealed that degradation performance did not improve beyond 4 mA/cm^2, highlighting the onset of mass transfer limitations and the occurrence of parasitic reactions such as oxygen evolution. The analysis of limiting current density confirmed that the process operated under mass transfer control, especially at elevated current densities. Energy

consumption analysis showed that MMO generally consumed less energy than BDD due to its lower cell potential requirements; however, when degradation performance is taken into account, BDD was identified as the more effective and energy-efficient electrode. While stainless steel provides better results than graphite as the cathode, likely due to its higher electrical conductivity, the flat surface of both materials suggests that surface morphology was not a major factor under the conditions tested. These findings underline the importance of optimizing operating parameters, not only to enhance degradation performance but also to ensure energy efficiency and economic feasibility in practical applications.

Supplementary Materials: The following supporting information can be downloaded at: https://www.mdpi.com/article/10.3390/pr14020184/s1, Table S1. Physicochemical characteristics of real tannery wastewater; Text S1. Experimental details of the limiting current technique; Text S2. Root-mean-square error (RMSE) and R^2 equations; Table S2. Electrode potentials from chronopotentiometry measurement; Table S3. Limiting current values from linear scan voltammetry measurement; Table S4. Kinetic rate constant along with RMSE and R^2 value at different applied current densities under multiple electrode pairings setup.

Author Contributions: Conceptualization, F.H.A.; methodology, N.N., F.H.A. and M.F.R.; software, N.N.; validation, F.H.A.; formal analysis, N.N.; investigation, N.N., M.F.R. and A.S.M.C.; resources, F.H.A. and A.S.M.C.; data curation, N.N. and F.H.A.; writing—original draft preparation, N.N.; writing—review and editing, F.H.A., M.U.M.J. and M.A.H.; visualization, N.N.; supervision, F.H.A., M.U.M.J. and M.A.H.; project administration, F.H.A. and M.U.M.J.; funding acquisition, F.H.A., M.U.M.J. and M.A.H. All authors have read and agreed to the published version of the manuscript.

Funding: This research was funded by Universiti Malaya Early Career Research grant, grant number BKP012-2023-ECR and Water Aid Foundation UAE International grant, grant number IF014-2023.

Data Availability Statement: Data is contained within the article or Supplementary Material.

Conflicts of Interest: The authors declare no conflicts of interest.

Abbreviations

The following abbreviations are used in this manuscript:

BDD	Boron-doped diamond
CER	Chlorine evolution reaction
CP	Chronopotentiometry
CV	Cyclic voltammetry
EC	Energy consumption
EO	Electro-oxidation
HER	Hydrogen evolution reaction
LSV	Linear scan voltammetry
MMO	Mixed-metal oxide
OC	Operational cost
OER	Oxygen evolution reaction
RCS	Reactive chlorine species
SS	Stainless steel
STW	Simulated tannery wastewater

References

1. Ali, H.Q.; Yasir, M.U.; Farooq, A.; Khan, M.; Salman, M.; Waqar, M. Tanneries impact on groundwater quality: A case study of Kasur city in Pakistan. *Environ. Monit. Assess.* **2022**, *194*, 823. [CrossRef]
2. Rai, D.; Sinha, S. Impact of different anode materials on electro-Fenton process and tannery wastewater treatment using sequential electro-Fenton and electrocoagulation. *Chemosphere* **2023**, *336*, 139225. [CrossRef]

3. Bhardwaj, A.; Kumar, S.; Singh, D. Tannery effluent treatment and its environmental impact: A review of current practices and emerging technologies. *Water Qual. Res. J.* **2023**, *58*, 128–152. [CrossRef]
4. Zhao, J.; Wu, Q.; Tang, Y.; Zhou, J.; Guo, H. Tannery wastewater treatment: Conventional and promising processes, an updated 20-year review. *J. Leather Sci. Eng.* **2022**, *4*, 10. [CrossRef]
5. He, Q.; Yao, K.; Sun, D.; Shi, B. Biodegradability of tannin-containing wastewater from leather industry. *Biodegradation* **2007**, *18*, 465–472. [CrossRef] [PubMed]
6. Lofrano, G.; Meric, S. A review on occurrence, measurement, toxicity and tannin removal processes from wastewaters. *Environ. Eng. Manag. J.* **2019**, *18*, 109–123. [CrossRef]
7. Garcia-Segura, S.; Ocon, J.D.; Chong, M.N. Electrochemical oxidation remediation of real wastewater effluents—A review. *Process Saf. Environ. Prot.* **2018**, *113*, 48–67. [CrossRef]
8. Feng, Y.; Yang, L.; Liu, J.; Logan, B.E. Electrochemical technologies for wastewater treatment and resource reclamation. *Environ. Sci. Water Res. Technol.* **2016**, *2*, 800–831. [CrossRef]
9. Martínez-Huitle, C.A.; Ferro, S. Electrochemical oxidation of organic pollutants for the wastewater treatment: Direct and indirect processes. *Chem. Soc. Rev.* **2006**, *35*, 1324–1340. [CrossRef]
10. Adnan, F.H.; Pons, M.N.; Mousset, E. Thin film microfluidic reactors in electrochemical advanced oxidation processes for wastewater treatment: A review on influencing parameters, scaling issues, and engineering considerations. *Electrochem. Sci. Adv.* **2023**, *3*, e2100210. [CrossRef]
11. Qin, T.; Yao, B.; Zhou, Y.Y.; Wu, C.C.; Li, C.W.; Ye, Z.Y.; Zhi, D.; Lam, S.S. The three-dimensional electrochemical processes for water and wastewater remediations: Mechanisms, affecting parameters, and applications. *J. Clean. Prod.* **2023**, *408*, 14. [CrossRef]
12. Buso, A.; Balbo, L.; Giomo, M.; Farnia, G.; Sandonà, G. Electrochemical Removal of Tannins from Aqueous Solutions. *Ind. Eng. Chem. Res.* **2000**, *39*, 494–499. [CrossRef]
13. Panizza, M.; Cerisola, G. Electrochemical oxidation as a final treatment of synthetic tannery wastewater. *Environ. Sci. Technol.* **2004**, *38*, 5470–5475. [CrossRef]
14. Costa, C.R.; Montilla, F.; Morallón, E.; Olivi, P. Electrochemical oxidation of synthetic tannery wastewater in chloride-free aqueous media. *J. Hazard. Mater.* **2010**, *180*, 429–435. [CrossRef]
15. Alsaffar, M.A.; Rahman, M.A.; Mageed, A.K.; Ali, S.A.K.; Lutfee, T.; Adnan, S.W.; Shakir, H.A.A. Electrochemical removal of dye from a tanning process industrial wastewater. *Chem. Pap.* **2023**, *77*, 6311–6318. [CrossRef]
16. Zou, J.; Peng, X.; Li, M.; Xiong, Y.; Wang, B.; Dong, F.; Wang, B. Electrochemical oxidation of COD from real textile wastewaters: Kinetic study and energy consumption. *Chemosphere* **2017**, *171*, 332–338. [CrossRef] [PubMed]
17. Doumbi, R.T.; Bertrand Noumi, G.; Ngobtchok, B.; Domga. Tannery wastewater treatment by electro-Fenton and electro-persulfate processes using graphite from used batteries as free-cost electrode materials. *Case Stud. Chem. Environ. Eng.* **2022**, *5*, 100190. [CrossRef]
18. Martínez-Huitle, C.A.; dos Santos, E.V.; de Araújo, D.M.; Panizza, M. Applicability of diamond electrode/anode to the electrochemical treatment of a real textile effluent. *J. Electroanal. Chem.* **2012**, *674*, 103–107. [CrossRef]
19. Du, X.; Oturan, M.A.; Zhou, M.; Belkessa, N.; Su, P.; Cai, J.; Trellu, C.; Mousset, E. Nanostructured electrodes for electrocatalytic advanced oxidation processes: From materials preparation to mechanisms understanding and wastewater treatment applications. *Appl. Catal. B Environ.* **2021**, *296*, 120332. [CrossRef]
20. Kusmierek, E. Semiconductor electrode materials applied in photoelectrocatalytic wastewater treatment—An overview. *Catalysts* **2020**, *10*, 439. [CrossRef]
21. Karthick, K.; Sam Sankar, S.; Kundu, S. Chapter 16—Transition metal-based nitrides for energy applications. In *Nanostructured, Functional, and Flexible Materials for Energy Conversion and Storage Systems*; Pandikumar, A., Rameshkumar, P., Eds.; Elsevier: Amsterdam, The Netherlands, 2020; pp. 493–515.
22. Faye, G.; Sibali, L.L. A Review on Characterization, Treatment, and Impact of Tannery Wastewater in Ethiopia. *Environ. Qual. Manag.* **2025**, *34*, e70015. [CrossRef]
23. Bravo-Yumi, N.; Villaseñor-Basulto, D.L.; Pérez-Segura, T.; Pacheco-Álvarez, M.A.; Picos-Benitez, A.; Rodriguez-Narvaez, O.M.; Peralta-Hernández, J.M. Comparison and statistical analysis for post-tanning synthetic wastewater degradation using different electrochemical processes. *Chem. Eng. Process.—Process Intensif.* **2021**, *159*, 108244. [CrossRef]
24. Maisuria, K.J.; Shah, K.A.; Rana, J.K. Removal of tannic acid and COD from synthetic tannery wastewater. *IOP Conf. Ser. Earth Environ. Sci.* **2022**, *1086*, 012035. [CrossRef]
25. Cañizares, P.; Martínez, L.; Paz, R.; Sáez, C.; Lobato, J.; Rodrigo, M.A. Treatment of Fenton-refractory olive oil mill wastes by electrochemical oxidation with boron-doped diamond anodes. *J. Chem. Technol. Biotechnol.* **2006**, *81*, 1331–1337. [CrossRef]
26. Anglada, Á.; Urtiaga, A.M.; Ortiz, I. Laboratory and pilot plant scale study on the electrochemical oxidation of landfill leachate. *J. Hazard. Mater.* **2010**, *181*, 729–735. [CrossRef]
27. Adnan, F.H.; Pons, M.-N.; Mousset, E. Mass transport evolution in microfluidic thin film electrochemical reactors: New correlations from millimetric to submillimetric interelectrode distances. *Electrochem. Commun.* **2021**, *130*, 107097. [CrossRef]

28. LaRowe, D.E.; Van Cappellen, P. Degradation of natural organic matter: A thermodynamic analysis. *Geochim. Et Cosmochim. Acta* **2011**, *75*, 2030–2042. [CrossRef]
29. Yuen, P.K.; Lau, C.M.D. Application of stoichiometric hydrogen atoms for balancing organic combustion reactions. *Chem. Teach. Int.* **2021**, *3*, 313–323. [CrossRef]
30. Mousset, E.; Puce, M.; Pons, M.-N. Advanced electro-oxidation with boron-doped diamond for acetaminophen removal from real wastewater in a microfluidic reactor: Kinetics and mass-transfer studies. *ChemElectroChem* **2019**, *6*, 2908–2916. [CrossRef]
31. Alagesan, J.; Jaisankar, M.; Muthuramalingam, S.; Mousset, E.; Chellam, P.V. Influence of number of azo bonds and mass transport limitations towards the elimination capacity of continuous electrochemical process for the removal of textile industrial dyes. *Chemosphere* **2021**, *262*, 128381. [CrossRef]
32. Panizza, M.; Kapalka, A.; Comninellis, C. Oxidation of organic pollutants on BDD anodes using modulated current electrolysis. *Electrochim. Acta* **2008**, *53*, 2289–2295. [CrossRef]
33. Panizza, M.; Michaud, P.A.; Cerisola, G.; Comninellis, C. Anodic oxidation of 2-naphthol at boron-doped diamond electrodes. *J. Electroanal. Chem.* **2001**, *507*, 206–214. [CrossRef]
34. Panizza, M.; Martinez-Huitle, C.A. Role of electrode materials for the anodic oxidation of a real landfill leachate—Comparison between Ti–Ru–Sn ternary oxide, PbO_2 and boron-doped diamond anode. *Chemosphere* **2013**, *90*, 1455–1460. [CrossRef]
35. Adnan, F.H.; Pontvianne, S.; Pons, M.-N.; Mousset, E. Role of anodically electrogenerated hydroxyl radicals in minimizing mineral cathodic electroprecipitation in the presence of hard water. *Electrochem. Commun.* **2023**, *150*, 107493. [CrossRef]
36. Abdel-Aziz, A.B.; Heakal, F.E.-T.; El Nashar, R.M.; Ghayad, I.M. Green synthesis and characterization of binary, ternary, and quaternary Ti/MMO anodes for chlorine and oxygen evolution reactions. *Sci. Rep.* **2024**, *14*, 9821. [CrossRef]
37. Liu, Y.-J.; Hu, C.-Y.; Lo, S.-L. Direct and indirect electrochemical oxidation of amine-containing pharmaceuticals using graphite electrodes. *J. Hazard. Mater.* **2019**, *366*, 592–605. [CrossRef]
38. Özbay, İ.; Polat, N. Electro-oxidation of woodworking wastewater by using boron-doped diamond electrode. *Int. J. Environ. Anal. Chem.* **2022**, *102*, 7659–7672. [CrossRef]
39. Groenen Serrano, K. Chapter 6—Indirect electrochemical oxidation using hydroxyl radical, active chlorine, and peroxodisulfate. In *Electrochemical Water and Wastewater Treatment*; Martínez-Huitle, C.A., Rodrigo, M.A., Scialdone, O., Eds.; Butterworth-Heinemann: Oxford, UK, 2018; pp. 133–164.
40. Yao, J.; Mei, Y.; Xia, G.; Lu, Y.; Xu, D.; Sun, N.; Wang, J.; Chen, J. Process optimization of electrochemical oxidation of ammonia to nitrogen for actual dyeing wastewater treatment. *Int. J. Environ. Res. Public Health* **2019**, *16*, 2931. [CrossRef] [PubMed]
41. Wang, Y.; Guo, X.; Li, J.; Yang, Y.; Lei, Z.; Zhang, Z. Efficient electrochemical removal of ammonia with various cathodes and Ti/RuO_2-Pt anode. *Open J. Appl. Sci.* **2012**, *02*, 241–247. [CrossRef]
42. De Laat, J.; Truong Le, G.; Legube, B. A comparative study of the effects of chloride, sulfate and nitrate ions on the rates of decomposition of H_2O_2 and organic compounds by Fe(II)/H_2O_2 and Fe(III)/H_2O_2. *Chemosphere* **2004**, *55*, 715–723. [CrossRef]
43. Huang, L.; Li, L.; Dong, W.; Liu, Y.; Hou, H. Removal of ammonia by OH radical in aqueous phase. *Environ. Sci. Technol.* **2008**, *42*, 8070–8075. [CrossRef] [PubMed]
44. Adnan, F.H.; Olorounto, O.-G.; Pontvianne, S.; Pons, M.-N.; Mousset, E. Importance of organic- and inorganic-based electro-precipitation on the advanced electro-oxidation efficiency towards reclaimed wastewater treatment in thin-film reactor—Mechanistic and modeling studies. *J. Environ. Chem. Eng.* **2024**, *12*, 114908. [CrossRef]
45. Bagastyo, A.Y.; Batstone, D.J.; Rabaey, K.; Radjenovic, J. Electrochemical oxidation of electrodialysed reverse osmosis concentrate on Ti/Pt–IrO_2, Ti/SnO_2–Sb and boron-doped diamond electrodes. *Water Res.* **2013**, *47*, 242–250. [CrossRef]
46. Bergmann, M.E.H.; Koparal, A.S.; Iourtchouk, T. Electrochemical Advanced Oxidation Processes, Formation of Halogenate and Perhalogenate Species: A Critical Review. *Crit. Rev. Environ. Sci. Technol.* **2014**, *44*, 348–390. [CrossRef]
47. Azizi, O.; Hubler, D.; Schrader, G.; Farrell, J.; Chaplin, B.P. Mechanism of Perchlorate Formation on Boron-Doped Diamond Film Anodes. *Environ. Sci. Technol.* **2011**, *45*, 10582–10590. [CrossRef]
48. Bergmann, M.E.H.; Rollin, J. Product and by-product formation in laboratory studies on disinfection electrolysis of water using boron-doped diamond anodes. *Catal. Today* **2007**, *124*, 198–203. [CrossRef]
49. Bergmann, M.E.H.; Rollin, J.; Iourtchouk, T. The occurrence of perchlorate during drinking water electrolysis using BDD anodes. *Electrochim. Acta* **2009**, *54*, 2102–2107. [CrossRef]
50. Lin, Z.; Yao, W.; Wang, Y.; Yu, G.; Deng, S.; Huang, J.; Wang, B. Perchlorate formation during the electro-peroxone treatment of chloride-containing water: Effects of operational parameters and control strategies. *Water Res.* **2016**, *88*, 691–702. [CrossRef]
51. DOE. *Environmental Quality (Industrial Effluent) Regulations 2009*; Ministry of Natural Resources And Environmental Sustainability: Putrajaya, Malaysia, 2025.
52. Santacruz, W.; Faria, J.; De Mello, R.; Boldrin, M.V.; Motheo, A.d.J. Comparative study of MMO and BDD anodes for electrochemical degradation of diuron in methanol medium. *Chemosphere* **2024**, *366*, 143517. [CrossRef] [PubMed]

53. Muddemann, T.; Neuber, R.; Haupt, D.; Graßl, T.; Issa, M.; Bienen, F.; Enstrup, M.; Möller, J.; Matthée, T.; Sievers, M.; et al. Improving the Treatment Efficiency and Lowering the Operating Costs of Electrochemical Advanced Oxidation Processes. *Processes* **2021**, *9*, 1482. [CrossRef]
54. Sopaj, F.; Oturan, N.; Pinson, J.; Podvorica, F.I.; Oturan, M.A. Effect of cathode material on electro-Fenton process efficiency for electrocatalytic mineralization of the antibiotic sulfamethazine. *Chem. Eng. J.* **2020**, *384*, 123249. [CrossRef]
55. Horváth-Gönczi, N.; Bagi, Z.; Szuhaj, M.; Rákhely, G.; Kovacs, K. Bioelectrochemical systems (BES) for biomethane production—Review. *Fermentation* **2023**, *9*, 610. [CrossRef]
56. Dihrab, S.; Sopian, K.; Zaharim, A. Membrane and bipolar plates materials for regenerative fuel cells. In Proceedings of the 8th WSEAS International Conference on Simulation, Modelling and Optimization (SMO '08), Santander, Spain, 23–25 September 2008; pp. 183–188.
57. Wei, R.; Pei, S.; Yu, Y.; Zhang, J.; Liu, Y.; You, S. Water Flow-Driven Coupling Process of Anodic Oxygen Evolution and Cathodic Oxygen Activation for Water Decontamination and Prevention of Chlorinated Byproducts. *Environ. Sci. Technol.* **2023**, *57*, 17404–17414. [CrossRef]
58. Shao, D.; Zhang, Y.; Lyu, W.; Zhang, X.; Tan, G.; Xu, H.; Yan, W. A modular functionalized anode for efficient electrochemical oxidation of wastewater: Inseparable synergy between OER anode and its magnetic auxiliary electrodes. *J. Hazard. Mater.* **2020**, *390*, 122174. [CrossRef]
59. Snowdon, M.R.; Rathod, S.; Fattahi, A.; Khan, A.; Bragg, L.M.; Liang, R.; Zhou, N.; Servos, M.R. Water purification and electrochemical oxidation: Meeting different targets with BDD and MMO anodes. *Environments* **2022**, *9*, 135. [CrossRef]

Disclaimer/Publisher's Note: The statements, opinions and data contained in all publications are solely those of the individual author(s) and contributor(s) and not of MDPI and/or the editor(s). MDPI and/or the editor(s) disclaim responsibility for any injury to people or property resulting from any ideas, methods, instructions or products referred to in the content.